The Astrophysical Journal Letters, 728:L22 (5pp), 2011 February 10 doi:10.1088/2041-8205/728/1/L22

PROBING VERY BRIGHT END OF GALAXY LUMINOSITY FUNCTION AT $z \gtrsim 7$ USING *HUBBLE SPACE TELESCOPE* PURE PARALLEL OBSERVATIONS*

Haojing Yan[1], Lin Yan[2], Michel A. Zamojski[2], Rogier A. Windhorst[3], Patrick J. McCarthy[4], Xiaohui Fan[5], Huub J. A. Röttgering[6], Anton M. Koekemoer[7], Brant E. Robertson[8,10], Romeel Davé[5], and Zheng Cai[9]
[1] Center for Cosmology and AstroParticle Physics, The Ohio State University, 191 West Woodruff Avenue, Columbus, OH 43210, USA
[2] Spitzer Science Center, California Institute of Technology, MS 220-6, Pasadena, CA 91125, USA
[3] School of Earth and Space Exploration, Arizona State University, Tempe, AZ 85287, USA
[4] Observatories of the Carnegie Institution of Washington, 813 Santa Barbara Street, Pasadena, CA 91101, USA
[5] Astronomy Department, The University of Arizona, Tucson, AZ 85721, USA
[6] Leiden Observatory, University of Leiden, P.O. Box 9513, Leiden 2300 RA, The Netherlands
[7] Space Telescope Science Institute, 3700 San Martin Drive, Baltimore, MD 21218, USA
[8] Astronomy Department, California Institute of Technology, MS 249-17, Pasadena, CA 91125, USA
[9] Physics Department, The University of Arizona, Tucson, AZ 85721, USA
Received 2010 October 11; accepted 2010 December 27; published 2011 January 24

ABSTRACT

We report the first results from the Hubble Infrared Pure Parallel Imaging Extragalactic Survey, which utilizes the pure parallel orbits of the *Hubble Space Telescope* to do deep imaging along a large number of random sightlines. To date, our analysis includes 26 widely separated fields observed by the Wide Field Camera 3, which amounts to 122.8 arcmin^2 in total area. We have found three bright Y_{098}-dropouts, which are candidate galaxies at $z \gtrsim 7.4$. One of these objects shows an indication of peculiar variability and its nature is uncertain. The other two objects are among the brightest candidate galaxies at these redshifts known to date ($L > 2L^*$). Such very luminous objects could be the progenitors of the high-mass Lyman break galaxies observed at lower redshifts (up to $z \sim 5$). While our sample is still limited in size, it is much less subject to the uncertainty caused by "cosmic variance" than other samples because it is derived using fields along many random sightlines. We find that the existence of the brightest candidate at $z \approx 7.4$ is not well explained by the current luminosity function (LF) estimates at $z \approx 8$. However, its inferred surface density could be explained by the prediction from the LFs at $z \approx 7$ if it belongs to the high-redshift tail of the galaxy population at $z \approx 7$.

Key words: cosmology: observations – galaxies: luminosity function, mass function

1. INTRODUCTION

The Wide Field Camera 3 (WFC3) on board the *Hubble Space Telescope* (*HST*) has begun breaking new grounds in our exploration of the early universe. Using the ultra-deep observations taken by the "HUDF09" program (PI: G. D. Illingworth), samples of candidate galaxies at $z \approx 7$ have been greatly enlarged (Oesch et al. 2010; Bunker et al. 2010; McLure et al. 2010; Yan et al. 2010a), and candidates have been found at $z \approx 8$ (Bouwens et al. 2010b; McLure et al. 2010; Yan et al. 2010a) and possibly out to $z \approx 10$ (Yan et al. 2010a; Bouwens et al. 2010c). The studies of the stellar populations of galaxies at $z \gtrsim 7$ are now underway (e.g., Bouwens et al. 2010a; Labbé et al. 2010a, 2010b; Finkelstein et al. 2010). The pencil-beam HUDF09 data are augmented by the shallower but 8× wider observations (Windhorst et al. 2010) of the WFC3 Early Release Science Program 2 (ERS2; PI: O'Connell), which provide us a unique opportunity to study the bright end of the luminosity function (LF) at $z \gtrsim 7$ because of the much increased sample size of bright candidates (Wilkins et al. 2010, 2011; Bouwens et al. 2010d; Yan et al. 2010b). Even with the ERS2 data, however, we are only barely able to probe the bright end at $L \sim L^*$. It is important to extend our investigation to the brighter regime, as it could be where the progenitors of the high stellar-mass ($\gtrsim 10^{10}\ M_\odot$) galaxies at $z \approx 6$–5 would locate (Yan et al. 2005). Such studies will need to survey larger areas, and preferably along different sightlines in order to reduce the bias caused by the underlying large-scale structures (a.k.a. "cosmic variance;" see, e.g., Robertson 2010).

Our Hubble Infrared Pure Parallel Imaging Extragalactic Survey, or "HIPPIES," was designed for this purpose. This program utilizes the unique "pure parallel" observing mode of *HST*, which enables simultaneous observations using instruments that are not doing the primary observations. As the pointings of the primary observations are drawn from a wide variety of programs of different objectives, the associated parallel observations are in effect observing completely random fields and hence are ideally suited for minimizing the impact of cosmic variance. In *HST* Cycle 17, there were two pure parallel programs using WFC3 as the imaging instrument, one led by our team (PID 11702, PI: H. Yan) and the other led by M. Trenti et al. (PID 11700; Trenti et al. 2011). Our program has been extended to the coming Cycle 18 (PID 12286). HIPPIES will incorporate the data from all these programs for its science objectives, one of which being addressing the very bright end of galaxy LF at $z \approx 7$ and beyond. Here, we report our initial results based on the data taken by the end of Cycle 17. Throughout this Letter, we use the following cosmological parameters: $\Omega_M = 0.27$, $\Omega_\Lambda = 0.73$, and $H_0 = 71$ km s^{-1} Mpc^{-1}. The quoted magnitudes are all in the AB system.

2. DATA DESCRIPTION

In Cycle 17, pure parallels were only allowed when the prime instrument was either the Cosmic Origins Spectrograph (COS) or the Space Telescope Imaging Spectrograph (STIS). Programs

* Based on observations made with the NASA/ESA *Hubble Space Telescope*, obtained at the Space Telescope Science Institute, which is operated by the Association of Universities for Research in Astronomy, Inc., under NASA contract NAS 5-26555. These observations are associated with programs 11700 and 11702.
[10] Hubble Fellow.

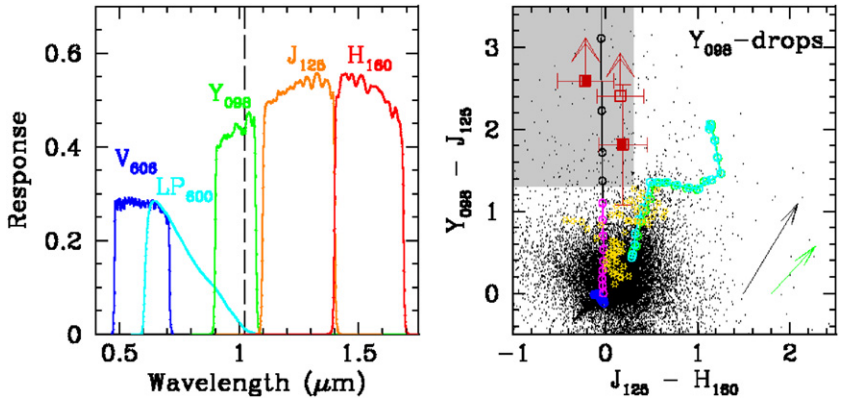

Figure 1. Left: system response curves of the WFC3 passbands used in the current pure parallel observations. Both programs used the same filters in the IR. In the UVIS, program 11700 used V_{606} while program 11702 used LP_{600}. The vertical dotted line indicates the location of Lyα line redshifted to $z = 7.4$. (right) Color–color diagram demonstrating the selection of Y_{098}-dropouts. The black dots are the field objects. The shaded area indicates the selection area, where the two objects in our final sample are shown in solid red squares and the peculiar Y_{098}-dropout that has an indication of variability is shown in open red square. The connected circles to left show the color track of a typical young galaxy at high redshifts using the model from Bruzual & Charlot (2003, (BC03); $\tau = 0.3$ Gyr and age of 100 Myr), and attenuated by the intervening H I absorption along the sightline using the formalism of Madau (1995). Different colors are used to code different redshift ranges along these tracks: blue is for $z < 6.4$, magenta is for $6.4 \leqslant z \leqslant 7.3$, and black is for $z \geqslant 7.4$. The selection area is well separated from the regions occupied by the potential sources of contaminations. The yellow stars show the colors of Galactic brown dwarfs (e.g., Leggett et al. 2002). The green symbols show the colors of a typical red galaxy at $z \approx 1$–3 simulated using a BC03 model ($\tau = 50$ Myr and age of 2.0 Gyr). The cyan symbols represent the colors of the same red galaxy but with a strong [O III] emission line of rest-frame equivalent width of 100 Å. The black and the green arrows represent the reddening vectors in these passbands appropriate for $z = 7.4$ and $z = 2$, respectively, using the reddening law of Calzetti (2001) and $E(B - V) = 0.5$ mag.

11700 and 11702 only requested the high galactic latitude opportunities at $|b| > 20^\circ$ and only requested long-duration opportunities ($\gtrsim$ 3 orbits) so that the observations could be sufficiently deep. The observations and data from these two programs are described below.

2.1. Observations

These two programs used both the infrared (IR) and the UV–optical (UVIS) channels of WFC3. The IR images were taken in the same three bands in both programs, namely, F098M, F125W, and F160W (hereafter Y_{098}, J_{105}, and H_{125}, respectively). In the UVIS channel, program 11700 used F606W (V_{606}), while program 11702 used F600LP (LP_{600}). The left panel of Figure 1 shows the system response curves in these passbands.

Our current work includes 26 WFC3 pure parallel fields acquired by the end of Cycle 17 (2010 August). The total exposure time in these fields ranges from 6 to 34 ks, with the median of 10.8 ks ($\sim$ 5 orbits). The distribution of exposure time in the four bands roughly follows the ratio of UVIS:F098M:F125W:F160W = 1:2:1:1, but varies significantly among the fields. The CCD observations in UVIS always have at least two CR-SPLIT exposures that enable the rejection of cosmic rays. Most of the IR observations also have at least two exposures each band in each field. As the IR array was always non-destructively read out multiple times during the exposure (at least five times for these observations), cosmic ray rejection generally is not a problem, even with single exposures.

2.2. Data Reduction

Our data reduction starts from the outputs from the *HST* On-the-Fly Reprocessing (OTFR) pipeline, which are photometrically calibrated images in units of count rate (i.e., the "*_flt.fits" images fetched from the *HST* data archive).

The vast majority of our parallel observations are non-dithered because the primary COS or STIS observations are not dithered. This makes it difficult to reject image defects using the usual outlier clipping method in the stacking process. Most of the defects are flagged in the "data quality" (DQ) extension of the processed image, which records the pixels that are diagnosed by the processing software to be problematic for various reasons (e.g., bad pixels, problems in telemetry, unstable response, etc.). In order to reduce their chance of contaminating our dropout sample, such image defects in the IR were filled by interpolation of nearby pixels. Using the archival ERS2 data, we also identified several thousands of additional outlier pixels that deviate from linear response at 5σ level, and these pixels were also fixed in the same way. The defected pixels were not treated for the UVIS images in the current work, because these images are only used for the "veto" purpose in the dropout selection, and hence such image defects in UVIS do not likely cause any contamination.

The MultiDrizzle software (Koekemoer et al. 2002) was then used to correct for the geometric distortions and to stack the images in each band. For each field, the World Coordinate System (WCS) of the first image in Y_{098} was always chosen as the reference to align all images. The final pixel scale that we adopted is $0\farcs09$ pixel^{-1}. The pixel noise of the drizzle-combined images is correlated at small scale because of the subpixel sampling. We followed the procedure utilized in the GOODS program (Dickinson et al. 2004) to calculate the correlation amplitudes in our mosaics, and then to derive the so-called RMS maps that register the absolute root-mean-square noise in each pixel.

2.3. Photometry

Matched-aperture photometry was carried out by running the SExtractor program of Bertin & Arnouts (1996) in dual-image mode. The J_{125}-band mosaics were used as the detection images. We adopt the SExtractor MAG_AUTO magnitudes, which were measured using the default (Kron factor, minimum radius) of (2.5, 3.5). A 2 pixel, 5 × 5 Gaussian filter was used to convolve the J_{125}-band images for detection; the detection threshold was set to 1.5σ, and a minimum of four connected pixels above the threshold was required. The RMS maps were used to measure the noise in the pixels within the MAG_AUTO apertures. We

Table 1
Properties of Y_{098}-Dropouts[a]

ID	R.A. and Decl. (J2000)[b]	V_{606}	LP_{600}	Y_{098}	J_{125}	H_{160}	$Y-J$	$J-H$
HIPPIES-YsDrop01	16:31:35.24 +37:36:14.03	> 28.1	···	27.33 ± 0.71	25.52 ± 0.16	25.33 ± 0.21	1.81	0.19
HIPPIES-YsDrop02	14:36:50.56 +50:43:33.69	> 28.4	···	> 28.4	25.86 ± 0.15	26.07 ± 0.27	> 2.5	-0.21
HIPPIES-YsDrop03[c]	07:50:51.41 +29:16:17.54	> 28.4	> 28.3	> 29.0	26.62 ± 0.17	26.46 ± 0.20	> 2.4	0.16

Notes.
[a] All magnitude limits are 2σ limits measured within an $r = 0\farcs2$ aperture.
[b] The quoted coordinates are based on the astrometric solutions provided by the OTFR pipeline for the first Y_{098} image in each field.
[c] This object shows indication of variability and thus its nature is unclear.

only include sources at S/N $\geqslant 5$ in the J_{125} band (within the MAG_AUTO aperture) for further analysis.

The depth of our mosaics varies significantly because the exposure time and the background condition vary significantly among the HIPPIES fields. For reference, the median 5σ depths measured within a $0\farcs2$ radius aperture are 27.36, 27.08, 27.16, 27.05, and 26.68 mag in V_{606}, LP_{600}, Y_{098}, J_{125}, and H_{160}, respectively. The source count at $J_{125} \leqslant 25.2$ mag is complete in every field and is complete at $J_{125} \leqslant 26.0$ mag for 20 out of the 26 fields.

3. CANDIDATE GALAXIES AT $z \gtrsim 7.4$

In this section, we describe the selection of candidate galaxies at $z \gtrsim 7.4$ as Y_{098}-dropouts using HIPPIES data.

3.1. Y_{098}-dropout Selection

Because Y_{098} does not overlap with J_{125}, it is possible to adopt a large color decrement such that the selection is less prone to the confusion with the 4000 Å break of red galaxies at low redshifts and less affected by photometric errors. Following Yan et al. (2010b), our main color criteria are $Y_{098} - J_{125} > 1.3$ mag and non-detections (i.e., S/N < 2) in the "veto" V_{606} and/or LP_{600} images. Based on our simulation using a large number of galaxy templates from the models of Bruzual & Charlot (2003) and the line-of-sight H I absorption recipe of Madau (1995), the adopted $Y_{098} - J_{125}$ color decrement is appropriate for selecting galaxies at $z \gtrsim 7.4$. As our UVIS images are not very deep, and we do not have data at longer wavelength (such as *Spitzer* IRAC data; see, e.g., Yan et al. 2010a, 2010b), we further require that a legitimate candidate should have $J_{125} - H_{160} < 0.3$ mag in order to further reduce the chance of contamination from red galaxies at low redshifts. The right panel of Figure 1 shows the selection of Y_{098}-dropouts on the $J_{125} - H_{160}$ versus $Y_{098} - J_{125}$ color–color diagram.

The selected candidates were visually inspected to exclude objects that were formally reported to have S/N < 2 in the UVIS image but still visible to eyes. In this step, we also rejected objects that were caused by artifacts and image defects that are not identified in the data reduction process (see Section 2.2). A last concern about the contamination is that the interpolation of the identified defected pixels might leave some residuals that could mimic the colors of Y_{098}-dropouts by chance. To deal with this problem, we created masks of the interpolated pixels (see Section 2.2) for the individual images and ran MultiDrizzle to project them to the same reference frame of the science images. The locations of the candidates were examined on these projected masks, and we only kept the objects that do not have any defects in the central 6×6 pixel area.

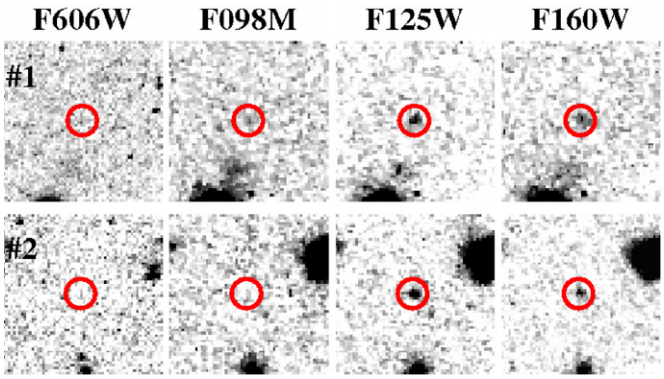

Figure 2. Image stamps of the two Y_{098}-dropouts in our sample. Images are $5\farcs4 \times 5\farcs4$ in size. The red circles are $0\farcs5$ in radius. North is up and east is to left.

3.2. Sample

Our selection above resulted in a total of three Y_{098}-dropouts over 26 HIPPIES fields that amount to 122.8 arcmin^2 in area. The colors of these three Y_{098}-dropouts are superposed in the right panel of Figure 1 (solid red squares). Their image are shown in Figures 2 and 3, and Table 1 lists their photometric information.

One of these three objects, YsDrop03 (see Figure 3), shows an indication of peculiar variability, which makes its candidacy as a high-redshift galaxy less certain. We performed photometry in each individual image and obtained its light curves as shown in Figure 3. The variability is the most obvious in H_{160}, where it is the brightest in the first image, declines by $\sim$1.0 mag within 2 days, and remains nearly constant in the following $\sim$1.2 days. Similar trend is also seen in J_{125}, albeit less significantly. However, such a variability does not seem to present in Y_{098} or the two UVIS bands, where this object always remains undetected although the observations in these bands were executed both before and after the first images were taken in H_{160} and J_{125}. Therefore, this object still remains a legitimate Y_{098}-dropout after this scrutiny. If it is not at $z \gtrsim 7.4$, the only viable explanation for its color and its variability is that it is a flaring brown dwarf star within our Galaxy (e.g., Schmidt et al. 2007). However, this interpretation is less favored, because this object has full width at half-maximum (FWHM) of $\sim 0\farcs3$ in both J_{125} and H_{160} stacks and hence seems to be resolved. Another possibility is that this object is an active galactic nucleus (AGN; see, e.g., Cohen et al. 2006) at $z \gtrsim 7.4$, or a transient at a similar redshift. Without further data, it is difficult to determine its nature. In any case, it does not fit in the conventional picture of a Lyman break galaxy (LBG), and therefore we do not include it in our final sample.

The remaining two are good candidate galaxies at $z \gtrsim 7.4$. None of them show time variability. Both are resolved (FWHM

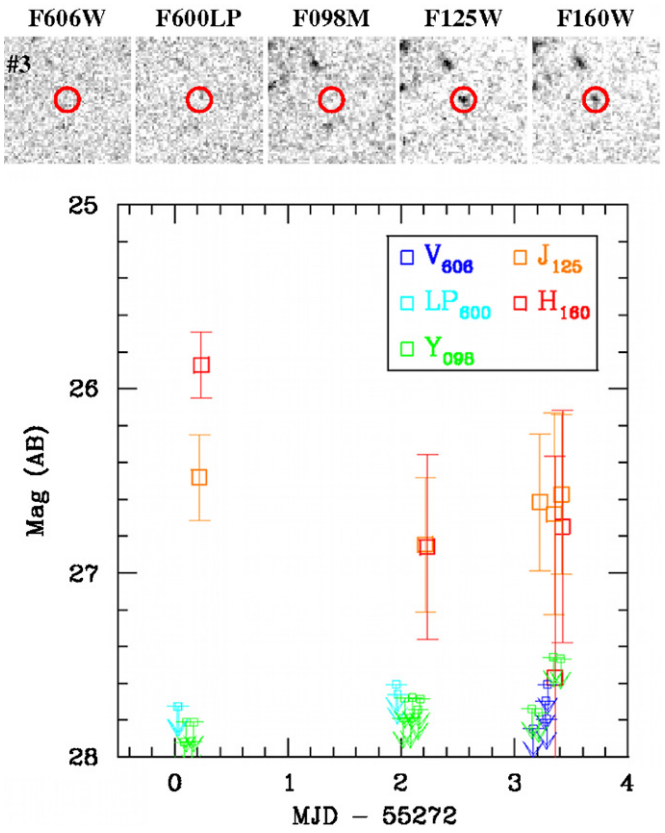

Figure 3. Top: same as Figure 2, but for the variable object (YsDrop03). The field was observed by both programs 11700 and 11702, and hence has UVIS data in both V_{606} and LP_{600}. Bottom: light curves of HIPPIES YsDrop03. The J_{125} and H_{160} data points are matched-aperture MAG_AUTO magnitudes obtained using the master J_{125} stack as the detection image, while the arrows are the 2σ upper limits measured within an $r = 0\farcs2$ aperture. The errors are 1σ error within the MAG_AUTO aperture.

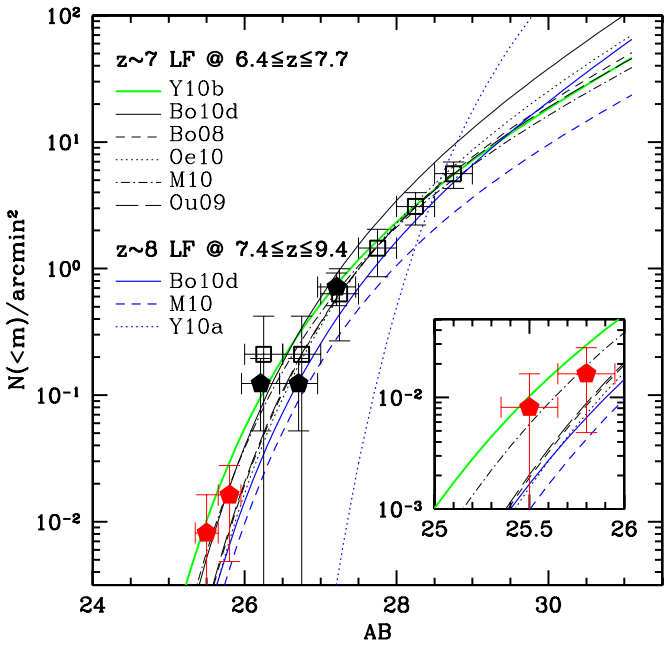

Figure 4. Comparison of the surface density of Y_{098}-dropouts at the very bright end inferred from our sample (red solid pentagons) and the predictions from various LFs at $z \approx 7$ and 8 (curves). The inset zooms in the region at the very bright end. The $z \approx 7$ LFs are taken from Bouwens et al. (2008, Bo08), Ouchi et al. (2009, Ou09), McLure et al. (2010, M10), Oesch et al. (2010, Oe10), Bouwens et al. (2010d, Bo10d), and Yan et al. (2010b, Y10b), while the $z \approx 8$ LFs are taken from Bo10d, M10, and Yan et al. (2010a, Y10a). The $z \approx 7$ LFs are integrated over $6.4 \leqslant z \leqslant 7.7$, while the $z \approx 8$ ones are integrated over $7.4 \leqslant z \leqslant 9.4$. The surface density of galaxies at $z \approx 7$ inferred from the z_{850}-dropouts in the HUDF (black open squares; Yan et al. 2010a) and the ERS2 field (black solid squares; Yan et al. 2010b) are also plotted.

$\gtrsim 0\farcs3$–$0\farcs4$) in J_{125} and H_{160} bands and hence are not likely brown dwarfs. Finally, they are not likely red galaxies at $z \approx 1$–3 whose 4000 Å break could mimic Lyman break, as their $J_{125}-H_{160}$ colors are much bluer than those of such interloppers. This is particularly true for YsDrop02, which has a very blue color of $J_{125} - H_{160} \approx -0.2$ mag. A few similar cases have already been observed in candidate galaxies at $z \approx 7$ and beyond (e.g., Oesch et al. 2010; Bouwens et al. 2010a; Yan et al. 2010a, 2010b).

4. DISCUSSION

The two Y_{098}-dropouts in our final sample are the brightest candidate galaxies at $z > 7$ discovered by WFC3 to date. Even assuming that their redshifts are at the lower end of the selection window ($z \approx 7.4$), we obtained their absolute magnitudes of $M = -21.6 \pm 0.16$ and -21.2 ± 0.15 mag for YsDrop01 and YsDrop02, respectively, which are at least $2\times$ brighter than any current estimates of the M^* value at $z \approx 7$ or 8. Earlier surveys over contiguous fields have resulted in a number of z-band dropouts (candidate galaxies at $z \approx 7$) of comparable brightness (e.g., Ouchi et al. 2009; Hickey et al. 2010; Castellano et al. 2010) or even brighter (Capak et al. 2009), and our current work indicates that such high luminosity galaxies could exist at $z \gtrsim 7.4$.

Using the formalism of Madau et al. (1998), the rest-frame UV luminosities of our candidates correspond to star formation rates (SFRs) of $23.7^{+3.5}_{-3.1}$ and $16.4^{+2.4}_{-2.1}$ $M_\odot$ yr^{-1}. As an order-of-magnitude estimate, if they keep forming stars at the same rates to $z \approx 5$, they could accumulate stellar masses of $(0.7\text{–}1.1) \times 10^{10}$ $M_\odot$ in the next ~473 million years. Therefore, our Y_{098}-dropouts could be the progenitors of the high-mass LBGs observed at $z \approx 5$ that have stellar masses to the order of $\sim 10^{10}$ $M_\odot$ (see, e.g., Yan et al. 2005; Stark et al. 2007).

The existing LF estimates of LBGs at $z \approx 7$ and beyond are largely based on observations at $L \lesssim L^*$. For this reason, it is interesting to see whether the number density of such very bright candidate galaxies at $z \gtrsim 7.4$ is consistent with the expectations from such LFs. This comparison is shown in Figure 4, where the result from this study is shown as the red pentagons. As the formal redshift selection window of Y_{098}-dropout spans $7.4 \lesssim z \lesssim 9.4$, we compare to the predictions from the LFs at both $z \approx 8$ and 7. Our data point is apparently higher than the predictions from the $z \approx 8$ LFs, including the one of Bo10d that predicts the highest surface density. If we single out the brightest object YsDrop01, the discrepancy is more obvious. The Bo10d $z \approx 8$ LF predicts a cumulative surface density of $\sim 2.7 \times 10^{-3}$ per arcmin^2 to $\leqslant 25.6$ mag over $7.4 \lesssim z \lesssim 9.4$, which is a factor of three lower than the density inferred from our YsDrop01 (8.1×10^{-3} per arcmin^{-2}). On the other hand, the LF of Yan et al. (2010b; $M^* = -20.33$, $\alpha = -1.80$ and $\Phi = 5.52 \times 10^{-4}$ Mpc^{-3}) predicts the highest bright-end surface density at $z \approx 7$. This LF, like others that are mostly based on the WFC3 z_{850}-dropout results, is applicable over the redshift range of $6.4 \lesssim z \lesssim 7.7$. It predicts a cumulative surface density of $\sim 1.5 \times 10^{-2}$ per arcmin^2 to $\leqslant 25.6$ mag, which

seems to be able to explain the existence of YsDrop01 if it is at $z \lesssim 7.7$.

5. SUMMARY

In this Letter, we present the initial results from the HIPPIES program. To date, our analysis includes 26 widely separated *HST* WFC3 pure parallel fields at $|b| > 20^{\circ}$ obtained in Cycle 17, which amount to 122.8 arcmin^2 in total area. Using these data, we search for candidate galaxies at $z \gtrsim 7.4$ as Y_{098}-dropouts. One candidate that we found shows an indication of peculiar variability in J_{125} and H_{160} but remains undetected in the bluer bands and its nature is unclear. Excluding this object, our current sample consists of two very bright candidates at $L > 2L^*$, which, based on their SFR estimates, could be linked to the progenitors of high-mass LBGs observed at lower redshifts (up to $z \sim 5$). While its size is still very limited, our sample is constructed from a large number of random fields and thus the impact of cosmic variance is minimal. The surface density inferred from our brightest candidate is not well explained by the existing LF estimates at $z \approx 8$, but could be explained by the prediction of LFs at $z \approx 7$ if it belongs to the high-redshift tail of the $z \approx 7$ galaxy population. Our new HIPPIES data soon to be taken in the coming *HST* cycle (∼42 pointings) will enable us to search for different Y_{105}-dropouts in a similar way, and the comparison of the two results will shed light to the evolution of the star formation activities in the early universe.

We thank the referee for the helpful comments. We acknowledge the support of NASA grant HST-GO-11702.*. H.Y. is supported by the long-term fellowship program of the Center for Cosmology and AstroParticle Physics (CCAPP) at The Ohio State University. B.E.R. is supported by Hubble Fellowship Program number HST-HF-51262.01-A. R.A.W. is supported by NASA JWST Interdisciplinary Scientist grant NAG5-12460 from GSFC. We dedicate this Letter to the memory of John Huchra, who during his life had been a very staunch supporter of the *Hubble Space Telescope* project.

REFERENCES

Bertin, E., & Arnouts, S. 1996, A&AS, 117, 393
Bouwens, R. J., Illingworth, G. D., Franx, M., & Ford, H. 2008, ApJ, 686, 230
Bouwens, R. J., et al. 2010a, ApJ, 708, L69
Bouwens, R. J., et al. 2010b, ApJ, 709, L133
Bouwens, R. J., et al. 2010c, Nature, submitted (arXiv:0912.4263)
Bouwens, R. J., et al. 2010d, ApJ, submitted (arXiv:1006.4360)
Bruzual, G., & Charlot, S. 2003, MNRAS, 344, 1000
Bunker, A., et al. 2010, MNRAS, 409, 855
Calzetti, D. 2001, PASP, 113, 1449
Capak, P., et al. 2009, arXiv:0910.0444
Castellano, M., et al. 2010, A&A, 524, 28
Cohen, S. H., et al. 2006, ApJ, 639, 731
Dickinson, M., et al. 2004, ApJ, 600, L99
Finkelstein, S. L., Papovich, C., Giavalisco, M., Reddy, N. A., Ferguson, H. C., Koekemoer, A. M., & Dickinson, M. 2010, ApJ, 719, 1250
Hickey, S., Bunker, A., Jarvis, M. J., Chiu, K., & Bonfield, D. 2010, MNRAS, 404, 212
Koekemoer, A. M., Fruchter, A. S., Hook, R. N., & Hack, W. 2002, in The 2002 HST Calibration Workshop: Hubble after the Installation of the ACS and the NICMOS Cooling System, ed. S. Arribas, A. Koekemoer, & B. Whitmore (Baltimore, MD: Space Telescope Science Institute), 337
Labbé, I., et al. 2010a, ApJ, 708, L26
Labbé, I., et al. 2010b, ApJ, 716, L103
Leggett, S. K., et al. 2002, ApJ, 564, 452
Madau, P. 1995, ApJ, 441, 18
Madau, P., Pozzetti, L., & Dickinson, M. 1998, ApJ, 498, 106
McLure, R. J., Dunlop, J. S., Cirasuolo, M., Koekemoer, A. M., Sabbi, E., Stark, D. P., Targett, T. A., & Ellis, R. S. 2010, MNRAS, 403, 960
Oesch, P. A., et al. 2010, ApJ, 709, L21
Ouchi, M., et al. 2009, ApJ, 706, 1136
Robertson, R. E. 2010, ApJ, 713, 1266
Schmidt, S. J., Cruz, K. L., Bongiorno, B. J., Liebert, J., & Reid, I. N. 2007, AJ, 133, 2258
Stark, D. P., Bunker, A. J., Ellis, R. S., Eyles, L. P., & Lacy, M. 2007, ApJ, 659, 84
Trenti, M., et al. 2011, ApJ, 727, L39
Wilkins, S. M., Bunker, A. J., Ellis, R. S., Stark, D., Stanway, E. R., Chiu, K., Lorenzoni, S., & Jarvis, M. J. 2010a, MNRAS, 403, 938
Wilkins, S. M., Bunker, A. J., Lorenzoni, S., & Caruana, J. 2010b, MNRAS, accepted (arXiv:1002.4866)
Windhorst, R. A., et al. 2010, ApJ, submitted (arXiv:1005.2776)
Yan, H., Windhorst, R., Hathi, N., Cohen, S., Ryan, R., O'Connell, R., & McCarthy, P. 2010a, Res. Astron. Astrophys., 10, 867
Yan, H., et al. 2005, ApJ, 634, 109
Yan, H., et al. 2010b, ApJ, submitted